Icarus 204 (2009) 663–671

Contents lists available at ScienceDirect

Icarus

journal homepage: www.elsevier.com/locate/icarus

Mid-infrared reflectance spectra and optical constants of six iron oxide/oxyhydroxide phases

Timothy D. Glotch [a,*], George R. Rossman [b]

[a] Stony Brook University, Stony Brook, NY 11794-2100, United States
[b] Division of Geological and Planetary Sciences, California Institute of Technology, Pasadena, CA 91125-2500, United States

ARTICLE INFO

Article history:
Received 23 April 2009
Revised 25 June 2009
Accepted 3 July 2009
Available online 28 July 2009

Keywords:
Spectroscopy
Infrared observations
Mars

ABSTRACT

We have determined the real and imaginary indices of refraction (n and k) for six iron oxide/oxyhydroxide phases—magnetite, maghemite, goethite, lepidocrocite, akaganéite, and ferrihydrite. A single crystal of magnetite was used to derive bulk n and k values from 100–2000 cm^{-1} (5–100 μm). Synthetic nanocrystalline samples of maghemite, goethite, lepidocrocite, akaganéite, and ferrihydrite were pressed into compact pellets used to determine bulk n and k values from 100–1200 cm^{-1} (8.33–100 μm). All values of n and k (the optical constants) were determined from specular reflectance spectra acquired at 2 cm^{-1} spectral sampling using classical Lorentz–Lorenz dispersion theory. In this paper, we present the optical constants of all six minerals and the oscillator parameters with which they were modeled. Use of these optical constants could aid in radiative transfer models of terrestrial dust as well as Mars, the Moon, and airless bodies in the Solar System.

1. Introduction

Iron oxide and oxyhydroxide minerals are some of the most important products of weathering of primary igneous iron-bearing minerals on Earth and Mars. They are important components of terrestrial and martian dust, and therefore contribute to the atmospheric radiative transfer on those bodies (Pollack et al., 1979; Morris et al., 1989; Bell et al., 1995; Prospero, 1999; Sokolik and Toon, 1999; Kandler et al., 2007). Iron oxide and oxyhydroxides have also been detected or suggested to occur on the Moon and other airless bodies throughout the Solar System (Williams and Gibson, 1972; Vilas et al., 1994). Their presence in meteorites (Kerridge et al., 1979; Tomeoka and Buseck, 1988; Keller et al., 1994; Brearley, 1995, 2006) suggests that they might be detectable via remote sensing methods on asteroids, comets, and interplanetary dust. In order to quantitatively interpret thermal infrared spectra of these objects, the real and imaginary indices of refraction (n and k) of these and other minerals must be determined and used in radiative transfer or other light scattering models such as the extended boundary condition method (EBCM) recently employed by Mishchenko et al. (2007a,b).

In this work, we determine the mid-infrared indices of refraction (also called optical constants) from bidirectional specular reflectance spectra. Optical constants of a magnetite (Fe_3O_4) single crystal were determined from 100 to 2000 cm^{-1}, while pressed pellets of other samples allowed determination of the optical constants between 200 and 1200 cm^{-1}. Pressed pellet samples are all derived from nanocystalline synthetic powders and include maghemite (γ-Fe_2O_3), goethite (α-FeOOH), akaganéite (β-FeOOH), lepidocrocite (γ-FeOOH), and 2-line ferrihydrite ($Fe_5HO_8{\cdot}4H_2O$). The optical constants are determined by applying classical Lorentz–Lorenz dispersion analysis to these laboratory reflectance spectra. The reflectance spectra, optical constants, and dispersion parameters used to calculate them from the spectra are presented.

2. Methods

2.1. Sample descriptions

The samples used for this study are summarized in Table 1. They consist of a magnetite single crystal, and synthetic powders of maghemite, goethite, akaganéite, lepidocrocite, and ferrihydrite. The magnetite crystal is from Cerro Huañaquino, Bolivia. The goethite (GTS2) and lepidocrocite (LPS2) powders are described by Morris and Lauer (1981) and Morris et al. (1985) and were loaned to us by R.V. Morris. They are both synthetic powders manufactured by Pfizer, Inc. Both powders are composed of acicular (blade-shaped) crystals with mean crystal sizes of 50 × 400 nm and 30 × 900 nm for the goethite and lepidocrocite, respectively. The akaganéite (AKG1) sample is described in detail by Glotch and Kraft (2008). It is composed of somatoidal (spindle-shaped) crystals with a mean size of ~150 nm in the long direction. The

* Corresponding author. Address: Department of Geosciences, Stony Brook University, Stony Brook, NY 11794-2100, United States. Fax: +1 631 632 8240.
E-mail address: tglotch@notes.cc.sunysb.edu (T.D. Glotch).

0019-1035/$ - see front matter © 2009 Elsevier Inc. All rights reserved.
doi:10.1016/j.icarus.2009.07.024

Table 1
Fe oxide/oxyhydroxide samples examined in this study.

Sample	Stoichiometric formula	Sample preparation	Crystal shape	Crystal size	Reference/origin
Magnetite MAG1	Fe_3O_4	Single crystal	Octahedron	5 mm	Brumado, Bahia, Brazil
Goethite GTS2	α-FeOOH	Powder pellet	Acicular	50 × 400 nm	Morris and Lauer (1981)
Lepidocrocite LPS2	γ-FeOOH	Powder pellet	Acicular	30 × 900 nm	Morris and Lauer (1981)
Akaganéite AKG1	β-FeOOH	Powder pellet	Somatoidal	150 nm[a]	Glotch and Kraft (2008)
Maghemite ISK1	γ-Fe_2O_3	Powder pellet	Acicular	337 × 53 nm	Rossman collection
Ferrihydrite FHYD2	$Fe_5O_7(OH)\cdot 4H_2O$	Powder pellet	Irregular	2–3 nm	Michel et al. (2007)

[a] Typical size in long direction.

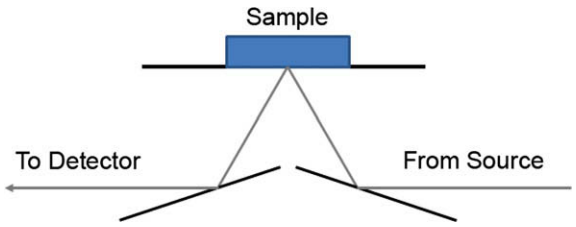

Fig. 1. Schematic of the FT-30 specular reflectance accessory used for all sample measurements. Angles of incidence and reflection are 30°.

maghemite powder was manufactured by ISK Magnetics and is part of the mineral collection of G.R. Rossman. It consists of acicular crystals with mean lengths and widths of 337 nm and 53 nm, respectively. The ferrihydrite is a synthetic powder that shows 2-lines in an XRD analysis, indicating that it is poorly ordered. It consists of irregularly shaped particles with diameters of 2–3 nm. The sample description and synthesis procedure is described by Michel et al. (2007). The sample was loaned to us by R. Harrington.

The single crystal of magnetite was polished to 1 μm roughness, providing a mirror-like surface, and ensuring specular reflectance at mid-to-far-IR wavelengths. The quality of the polish was checked with an optical microscope. Powdered samples were pressed into compact pellets at 15,000 psi using a Carver hydraulic press and a Pike Technologies 13 mm die kit. The resulting pellets had highly reflective surfaces, with the exception of ferrihydrite, which had a matte-like finish, resulting in a low sample reflectance.

2.2. Collection and processing of spectra

Mid-infrared (MIR) reflectance spectra (400–4000 cm^{-1}; 2.5–25 μm) were acquired on Stony Brook University's Nicolet 6700 Fourier Transform Infrared (FTIR) spectrometer at 2 cm^{-1}

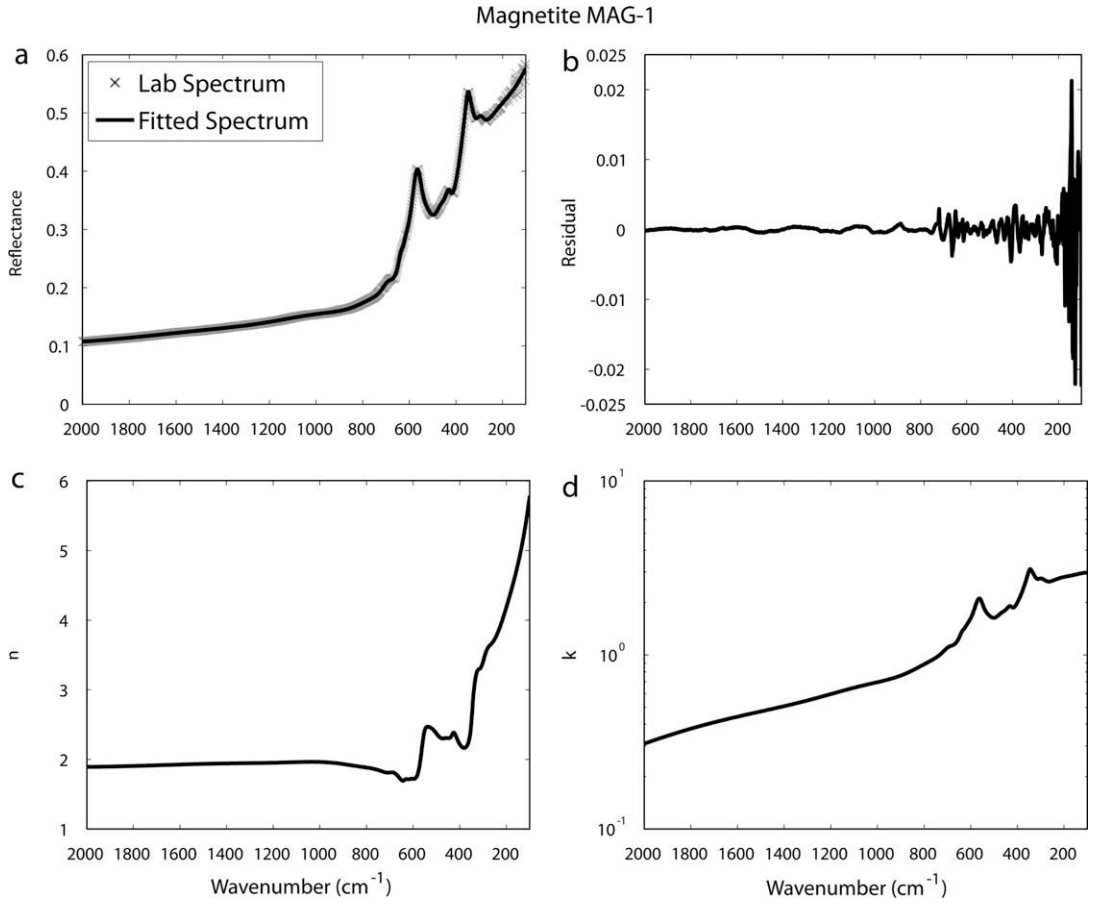

Fig. 2. Optical constant data for magnetite MAG1 including: (a) laboratory and modeled spectra, (b) residual of model fit, (c) real index of refraction, (d) imaginary index of refraction.

spectral sampling and in an atmosphere purged of H_2O and CO_2. The spectrometer is equipped with a Baseline FT-30 specular reflectance accessory with incidence and reflection angles of 30°. A schematic of the reflectance accessory is shown in Fig. 1. For collection of MIR spectra, the spectrometer is equipped with a KBr beamsplitter and a thermoelectrically cooled deuterated L-alanine doped triglycine sulfate (DLaTGS) detector with a KBr window. Far infrared (FIR) spectra (50–600 cm^{-1}; 16.67–200 μm) are collected with the same instrument using a Solid Substrate beamsplitter and a DTGS detector with a polyethylene window. A total of 512 scans were averaged for each MIR spectrum and 1024 scans were averaged to create each FIR spectrum. For several reasons (discussed below) pellet spectra are only modeled over the 100–1200 cm^{-1} range.

Both MIR and FIR spectra are referenced to a first-surface protected gold mirror. Because this mirror does not have a reflectance of unity, we determined the "reflectance function" of the instrument to remove the effects of non-unit reflectivity. This process involves several steps: (1) For both the MIR and FIR spectrometer setups, the reflectance accessory was removed from the spectrometer providing an unimpeded path from the modulated IR beam to the detector. A spectrum of the unimpeded beam was acquired as a background measurement. (2) The reflectance accessory was then inserted into the spectrometer along with the gold reflectance standard. We then acquired a spectrum of the standard using the spectrum acquired in step 1 as the background. It is the spectrum of the standard that we refer to as the instrument reflectance function. (3) Samples were placed on an aluminum aperture mask painted with Krylon ultra-black paint. The underside of the aperture mask was scored with 100 μm sandpaper and coated with black paraffin soot to further reduce its reflectance. Spectra were acquired of each sample placed on the aperture mask. (4) A spectrum of the empty mask was acquired as a "blank." (5) Each blank and sample spectrum was multiplied by the instrument reflectance function to cancel out the effects of non-unit reflectivity of the reflectance standard. (6) The corrected blank spectra were subtracted from the corrected sample spectra to arrive at the final fully processed spectra suitable for modeling.

MIR and FIR spectra of each sample were collected separately and merged near 500 cm^{-1}. Occasionally, there are small differences (~1–3%) in the spectral contrast between the MIR and FIR spectra, perhaps due to measurement of slightly different spots on the sample. In these cases, the FIR spectra are multiplicatively scaled to exhibit the same spectral contrast as the MIR spectra before they were merged together. Glotch et al. (2007) showed that measurement errors for a similar laboratory arrangement were ≪1% over the wavelength range utilized in this study, with a maximum error of ~3% of the maximum spectral contrast near 1050 cm^{-1}. Errors also tended to be higher (1–2%) at <300 cm^{-1}, where SNR degrades. In general, there is great reproducibility of reflectance spectra with current laboratory equipment, lending confidence to the derived optical constants.

Spectra of pressed pellets were modeled from 200 to 1200 cm^{-1}. This is due to the fact that at higher wavenumbers, the assumption of specular reflection from the pressed pellets becomes less valid. Additionally, the oxyhydroxide samples contain several minor spectral features between 1200 and 2000 cm^{-1} that are not well-accounted for by our model. At low wavenumbers, where the detector sensitivity is lowest, the pellets are not reflective enough to provide adequate signal.

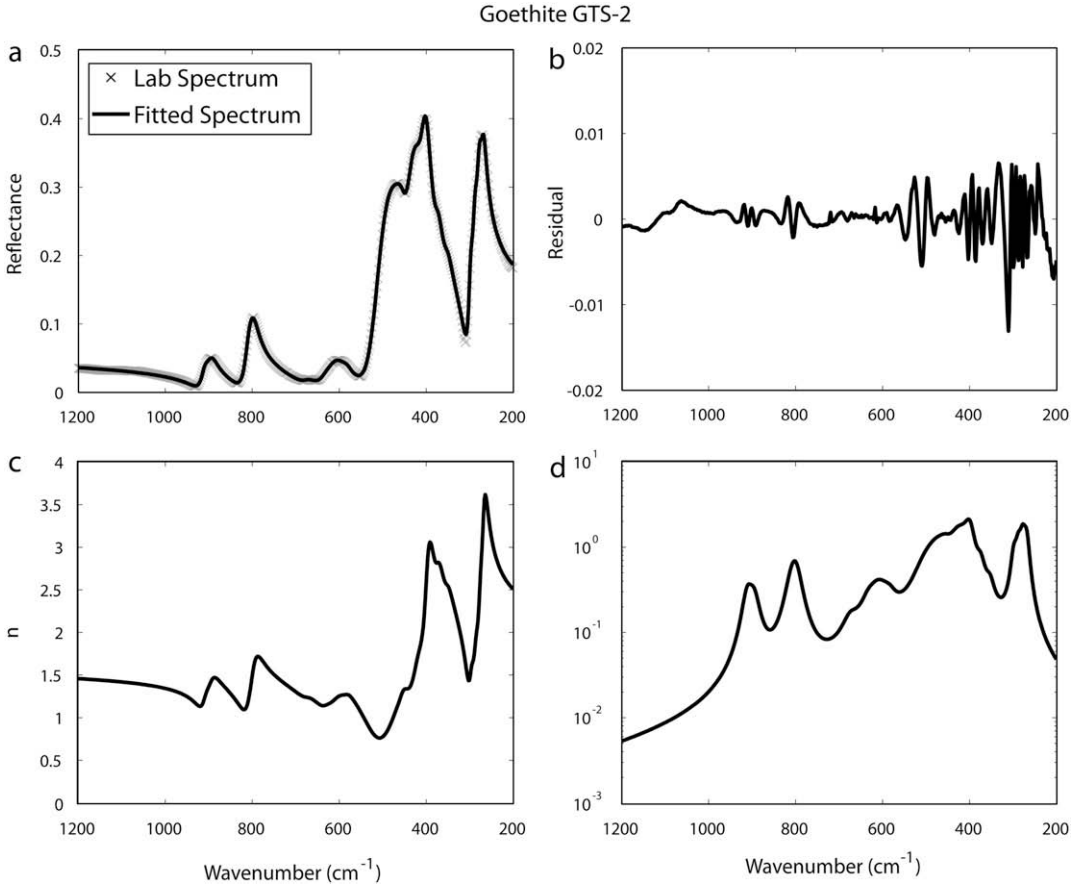

Fig. 3. Optical constant data for goethite GTS2 including: (a) laboratory and modeled spectra, (b) residual of model fit, (c) real index of refraction, (d) imaginary index of refraction.

2.3. Modeling of optical constants

To model the optical constants of the oxide/oxyhydroxide minerals described above, we make use of dispersion theory in combination with a Fresnel reflectance model using a nonlinear least squares optimization routine. Mineral spectra are iteratively fit with a modeled spectrum produced using dispersion and Fresnel equations. The real (n) and imaginary (k) indices of refraction are determined when the best fit between the measured and modeled spectra is achieved.

Each oscillator in a dispersion model is defined by three parameters: ν, $4\pi\rho$, and γ, which represent the center frequency of the oscillation, the band strength, and width, respectively. An additional term, ε_0, is the high frequency dielectric constant, which is a bulk mineral property rather than an oscillator-dependent property and should be equal to n^2_{vis} measured in the visible part of the spectrum (Roush et al., 1991). We use the dispersion theory formulation of Spitzer and Kleinman (1961) (Eqs. (1) and (2)) and combine it with a nonlinear least squares optimization routine described by Glotch et al. (2007).

$$n^2 - k^2 = \varepsilon_0 + \sum_j \frac{4\pi\rho_j \nu_j^2(\nu_j^2 - \nu^2)}{(\nu_j^2 - \nu^2)^2 + (\gamma_j^2 \nu_j^2 \nu^2)}, \quad (1)$$

$$nk = \sum_j \frac{2\pi\rho_j \nu_j^2(\gamma_j \nu_j \nu)}{(\nu_j^2 - \nu^2)^2 + (\gamma_j^2 \nu_j^2 \nu^2)}, \quad (2)$$

where j represents the jth oscillator and the strength ρ is defined as

$$\rho_j = \frac{Ne^2}{4\pi m^* \nu_j^2}, \quad (3)$$

where N is the concentration of ion pairs, e is the charge, and m^* is the reduced mass (Spitzer et al., 1959).

3. Results

The measured and modeled spectra of each sample, the residual between them, and the modeled values of n and k derived from the dispersion analysis are shown in Figs. 2–7. All measured and modeled spectra as well as the derived values of n and k can be accessed at http://www.ms.cc.sunysb.edu/~tglotch/optical_constants.htm or by contacting the first author.

The measured and modeled reflectance spectra and the optical constants of magnetite (MAG1) and goethite (GTS2) are shown in Figs. 2 and 3 and the oscillator parameters used to fit the reflectance spectra are shown in Table 2. The magnetite model required 15 oscillators to adequately model the MAG1 spectrum, while the goethite model required 17 oscillators to adequately model the GTS2 spectrum.

The measured and modeled reflectance spectra and the optical constants of lepidocrocite (LPS2) and akaganéite (AKG1) are shown in Figs. 4 and 5 and the oscillator parameters used to fit the reflectance spectra are shown in Table 3. The lepidocrocite model required 14 oscillators to adequately model the LPS2 spectrum,

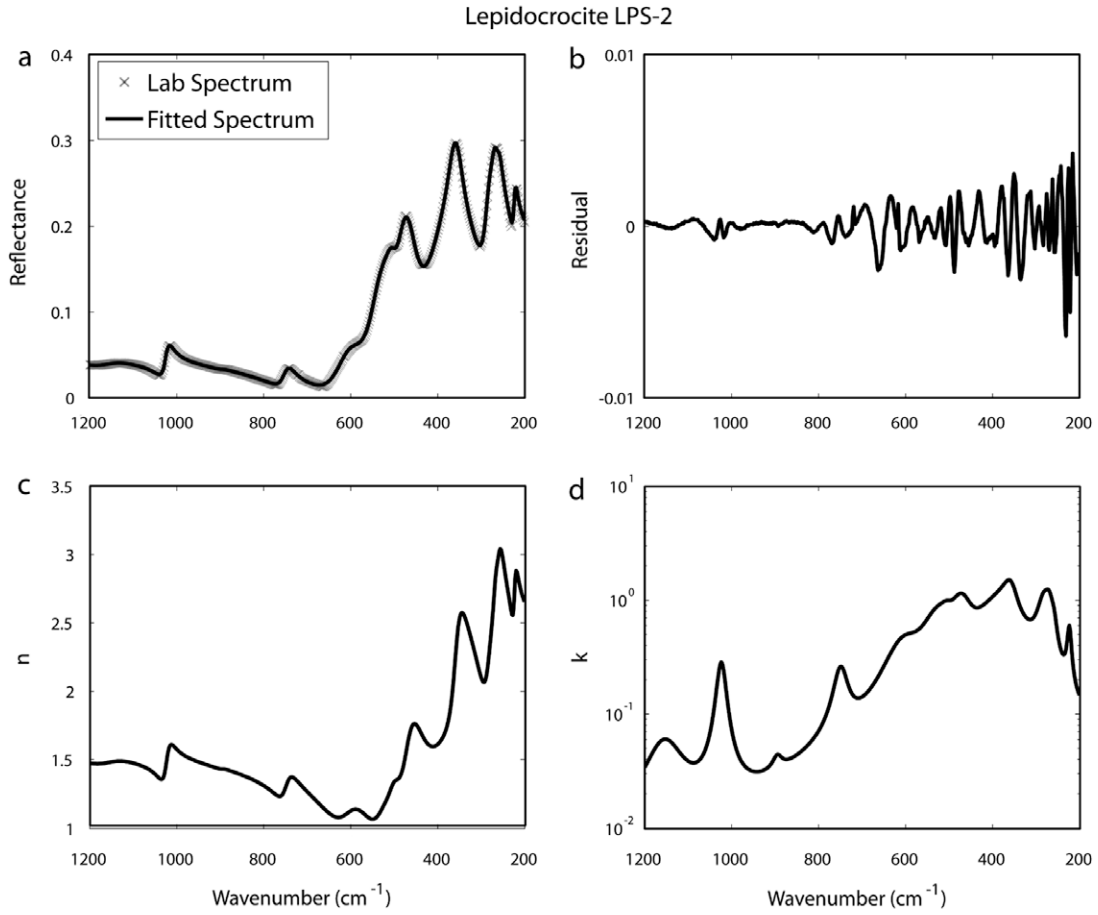

Fig. 4. Optical constant data for lepidocrocite LPS2 including: (a) laboratory and modeled spectra, (b) residual of model fit, (c) real index of refraction, (d) imaginary index of refraction.

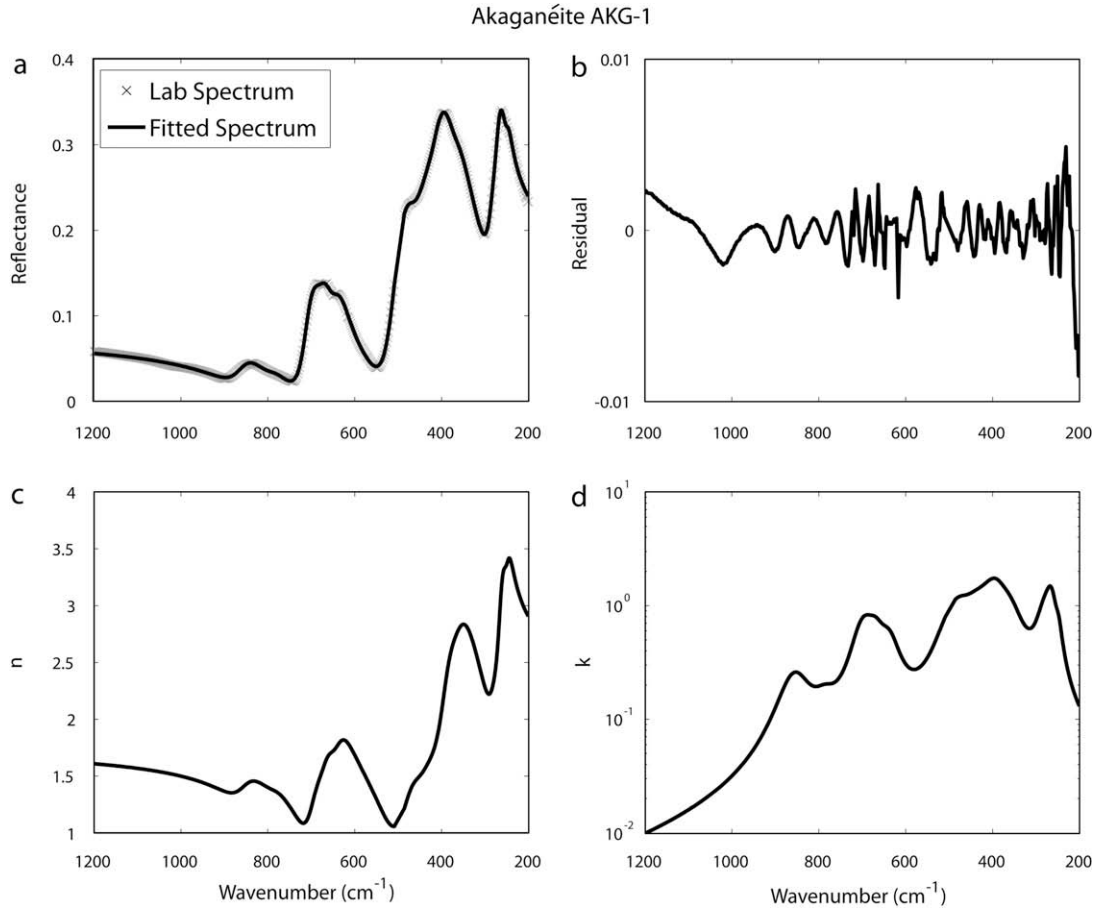

Fig. 5. Optical constant data for akaganéite AKG1 including: (a) laboratory and modeled spectra, (b) residual of model fit, (c) real index of refraction, (d) imaginary index of refraction.

while the akaganéite model required 12 oscillators to adequately model the AKG1 spectrum.

The measured and modeled reflectance spectra and the optical constants of maghemite (ISK1) and ferrihydrite (FHYD2) are shown in Figs. 6 and 7 and the oscillator parameters used to fit the reflectance spectra are shown in Table 4. The maghemite model required 27 oscillators to adequately model the ISK1 spectrum, while the ferrihydrite required eight oscillators to adequately model the FHYD2 spectrum.

4. Discussion

4.1. Optical constants measured from pressed powder pellets

Ideally, optical constants are obtained from polarized spectra measured of highly polished single crystals that are oriented parallel to the crystal axes (e.g. Spitzer and Kleinman, 1961; Long et al., 1993; Lane, 1999). In some cases, as for five of the six samples described in this work, it is not possible to obtain single crystals larger than ~5 mm (required by our spectrometer setup) for polarized IR spectral analysis. In these cases, optical constants derived from pressed powder pellets represent an adequate alternative. Long et al. (1993) performed classical dispersion analysis on spectra obtained of both single crystal and powder pellets of calcite and gypsum. Their analysis indicates that optical constants derived from spectra of pellets are within about a factor of 2 of those derived from single crystals. This is mainly due to the fact that spectra of pressed pellets have lower reflectance values than single crystals. In terms of the oscillator parameters used in the model, the lower reflectance translates to lower values of ε_0 (high frequency dielectric constant) and $4\pi\rho$ (oscillator strength) and an increase in γ (width) due to the larger full width at half maximum (Long et al., 1993). For the samples measured in this study, it is expected that optical constants derived from the ferrihydrite (FHYD2) pellet with a matte finish surface are not as close to "truth" as those derived from the highly reflective pellets.

An additional drawback of determining optical constants from powdered pellets is that they represent the "bulk" properties of the minerals in question. That is, the optical anisotropy of the samples cannot be modeled using polarized IR spectral analysis. The exception for the powder pellets analyzed in this study is maghemite, which is optically isotropic (Greenwood, 1970; Pecharromán et al., 1995).

4.2. Comparison with previous work

The optical constants of most of the minerals presented in this paper have not been previously modeled. While hematite (α-Fe_2O_3) has been the focus of several studies (Popova et al., 1973; Onari et al., 1977; Glotch et al., 2006) other iron oxide/oxyhydroxide minerals have received relatively little attention. The extinction coefficient (related to n and k) of magnetite from ~2.5–100 μm was presented by Koike et al. (1981), but not information on the nature of the sample or the experimental conditions was given. Optical constants for magnetite from 0.14 to 300 μm are listed in table format by Mukai (1986). Again, however, there is no information regarding the sample characteristics, the measurement conditions, or the method of optical constant derivation.

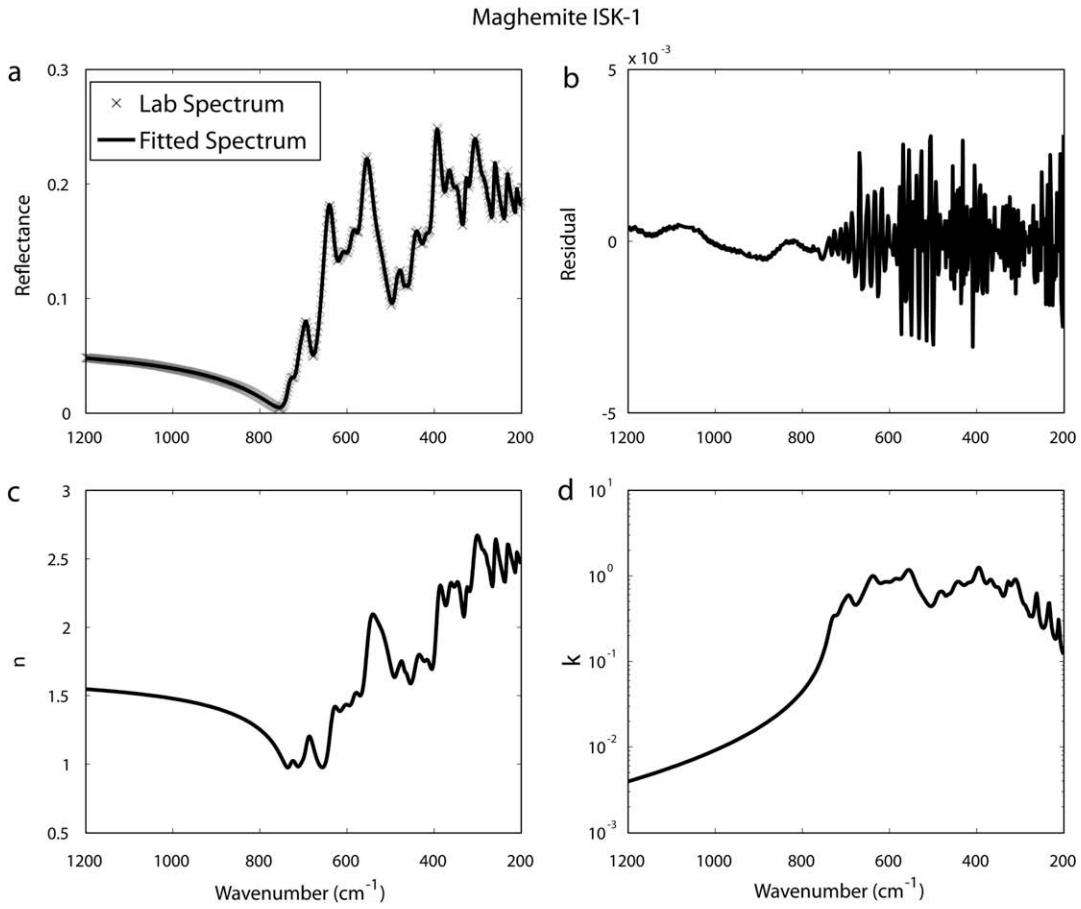

Fig. 6. Optical constant data for maghemite ISK1 including: (a) laboratory and modeled spectra, (b) residual of model fit, (c) real index of refraction, (d) imaginary index of refraction.

Comparison of the Mukai (1986) data with that presented in this work (Fig. 8) shows significant deviation in the magnitude and shape of the optical constant spectra between 100 and 2000 cm^{-1}. These differences could be due to sample size, composition, and/or preparation.

Pecharromán et al. (1995) determined the optical constants of several maghemite samples from pressed powder pellets. The samples examined by Pecharromán et al. (1995) varied greatly in their crystallinity and the positions of octahedral vacancies in the mineral crystal structures. The maghemite sample examined in this work most closely matches Sample 8 of Pecharromán et al. (1995) which shows a high degree of crystallinity. Using the model and oscillator parameters of Pecharromán et al. (1995), we have plotted the resulting optical constants of Sample 8 along with our maghemite sample ISK1. The results are shown in Fig. 9. The modeled optical constants of Pecharromán et al. (1995) are a factor of ~2.5 higher than those determined in this study. Pecharromán et al. (1995) modeled a pressed pellet of maghemite as a mixture of maghemite crystal spheres and air using effective medium theory (Landauer, 1978). This model uses assumptions of the particles' depolarization factors as well as volume fraction of particles within the pellet. In practice, the assumption of a significant fraction of air in the pellet (46% by volume assumed for Pecharromán Sample 8) has the effect of increasing the values of the optical constants needed to accurately model the reflectance spectrum of the pellet.

Optical constants of an aqueous goethite suspension were determined using variable angle attenuated total reflectance (ATR) spectroscopy and Kramers–Kronig modeling (Tickanen et al., 1997). These results, however, are not appropriate for comparison to dry bulk goethite. Optical constants of all other minerals discussed in this work have not been previously reported in the literature.

4.3. Application to Mars and other planetary bodies

Models based on radiative transfer are used to determine the scattering properties of fine particulates in planetary regoliths, which are present in the atmosphere and on the surface of Mars. Determination of the composition of these fine-grained surfaces throughout the Solar System remains a difficult problem due to the lack of appropriate optical constants of relevant materials. Perhaps the best example of such a problem is determining the mineralogical composition of the globally homogenous martian dust. This dust component, both entrained in the atmosphere and deposited on the classically bright regions of Mars, has been the subject of numerous studies (e.g. Toon et al., 1977; Pollack et al., 1979; Singer, 1982; Clancy et al., 1995; Bell et al., 2000; Murchie et al., 2000; Bishop et al., 2002; Hamilton et al., 2005) that have fostered significant discussion about the composition of the dust. Based on radiative transfer modeling and comparison to Mariner 9 IRIS spectra acquired during the 1971–1972 dust storm, Toon et al. (1977) concluded that the dust was composed primarily of weathering products of felsic rock components with SiO_2 >60%, and a secondary component such as basalt. Pollack et al. (1979) suggested that a minor magnetite component in the dust would be consistent with visible and ultraviolet dust absorptions. The presence of magnetite in the martian surface dust appears to have been confirmed by the magnetic properties experiment on the MER

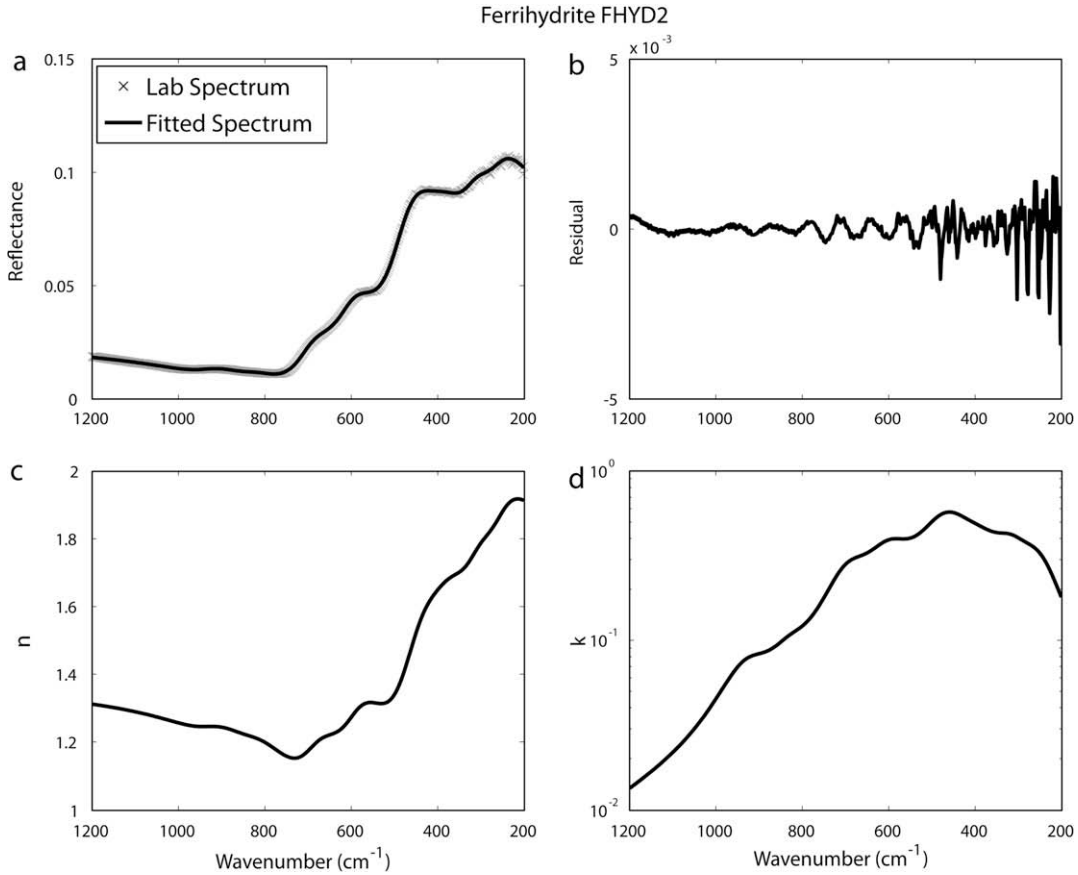

Fig. 7. Optical constant data for ferrihydrite FHYD2 including: (a) laboratory and modeled spectra, (b) residual of model fit, (c) real index of refraction, (d) imaginary index of refraction.

Table 2
Derived oscillator parameters for magnetite and goethite.

Magnetite MAG1 $\varepsilon_0 = 4.1778$			Goethite GTS2 $\varepsilon_0 = 2.4991$		
ν (cm^{-1})	γ	$4\pi\rho$	ν (cm^{-1})	γ	$4\pi\rho$
135	2.1764	33.8797	268	0.0505	0.3974
268	1.1106	8.9758	276	0.0501	0.2610
293	0.1477	0.3104	287	0.0507	0.1343
336	0.1564	0.7450	297	0.0433	0.0612
344	0.0623	0.1154	353	0.0587	0.0506
431	0.0678	0.0620	374	0.0596	0.1248
462	0.1635	0.2123	398	0.0579	0.4917
532	0.1922	0.4379	420	0.1008	0.3504
559	0.0819	0.2582	454	0.0591	0.0375
612	0.0855	0.0486	466	0.1513	0.2845
635	0.0402	0.0116	582	0.0470	0.0065
692	0.1031	0.0433	608	0.1108	0.0842
770	0.3523	0.2357	632	0.0426	0.0032
1049	0.7096	0.6783	674	0.0590	0.0085
1747	1.0689	1.1531	799	0.0391	0.0765
			895	0.0328	0.0215
			909	0.0265	0.0130

Table 3
Derived oscillator parameters for lepidocrocite and akaganéite.

Lepidocrocite LPS2 $\varepsilon_0 = 2.5969$			Akaganéite AKG1 $\varepsilon_0 = 3.0708$		
ν (cm^{-1})	γ	$4\pi\rho$	ν (cm^{-1})	γ	$4\pi\rho$
223	0.0469	0.1051	248	0.0645	0.1299
259	0.0633	0.1094	264	0.0953	0.4801
269	0.0732	0.2138	280	0.1438	0.3406
281	0.1082	0.3026	360	0.1831	0.5851
356	0.0968	0.3569	390	0.1625	0.8689
379	0.3821	1.1177	436	0.1745	0.2533
467	0.1057	0.2312	475	0.1411	0.2250
504	0.0637	0.0297	637	0.0847	0.1101
524	0.1306	0.1102	668	0.0650	0.0689
602	0.1520	0.0927	692	0.0762	0.0922
748	0.0464	0.0228	786	0.0762	0.0116
895	0.0281	0.0008	854	0.0944	0.0552
1023	0.0229	0.0181			
1154	0.0798	0.0113			

Spirit rover (Bertelsen et al., 2004). Later work by Clancy et al. (1995) indicated that the martian dust spectrum may be more consistent with the major component being palagonite, a weathering product of basaltic glass. This result is consistent with previous visible/near-IR observations (Allen et al., 1981; Singer, 1982) and later mid-IR observations (Morris et al., 2003).

The iron oxide and oxyhydroxide optical constants presented in this paper will enable more detailed modeling of the optical properties of the martian surface as well as the Moon and asteroids (Williams and Gibson, 1972; Vilas et al., 1994). Future work to determine the optical constants of a variety of silicates, including plagioclase feldspar, pyroxenes, and a range of olivine compositions will also make future compositional modeling efforts more robust.

5. Conclusions

We have acquired mid-IR reflectance spectra of a magnetite single crystal (100–2000 cm^{-1}) and pressed powder pellets of goethite, lepidocrocite, akaganéite, maghemite, and ferrihydrite

Table 4
Derived oscillator parameters for maghemite and ferrihydrite.

Maghemite ISK1 $\varepsilon_0 = 2.7679$			Ferrihydrite FHYD2 $\varepsilon_0 = 1.9390$		
ν (cm^{-1})	γ	$4\pi\rho$	ν (cm^{-1})	γ	$4\pi\rho$
212	0.0278	0.0237	260	0.4766	0.3521
234	0.0391	0.0646	321	0.3371	0.1888
258	0.9621	0.5464	390	0.3446	0.1695
262	0.0368	0.0779	462	0.3353	0.4057
275	0.0171	0.0033	597	0.2328	0.1218
282	0.0200	0.0046	692	0.1944	0.0681
288	0.0365	0.0169	830	0.1354	0.0075
309	0.0877	0.3155	930	0.1581	0.0148
327	0.0319	0.0486			
349	0.0580	0.0853			
366	0.0613	0.1398			
393	0.0621	0.2475			
419	0.0581	0.0573			
442	0.0789	0.1597			
465	0.0279	0.0080			
476	0.0285	0.0132			
485	0.0468	0.0442			
526	0.0846	0.0688			
552	0.0629	0.2162			
584	0.0484	0.0525			
608	0.0635	0.0722			
635	0.0408	0.0549			
645	0.1110	0.0658			
691	0.0259	0.0121			
702	0.0550	0.0290			
729	0.0296	0.0079			

(200–1200 cm^{-1}). We used the Spitzer and Kleinman (1961) formulation of Lorentz–Lorenz dispersion theory to model the optical constants of these minerals from the reflectance spectra. The optical constants determined in this work may aid in future studies of radiative transfer of terrestrial dust and modeling remote sensing data acquired of Mars, the Moon, and other airless bodies.

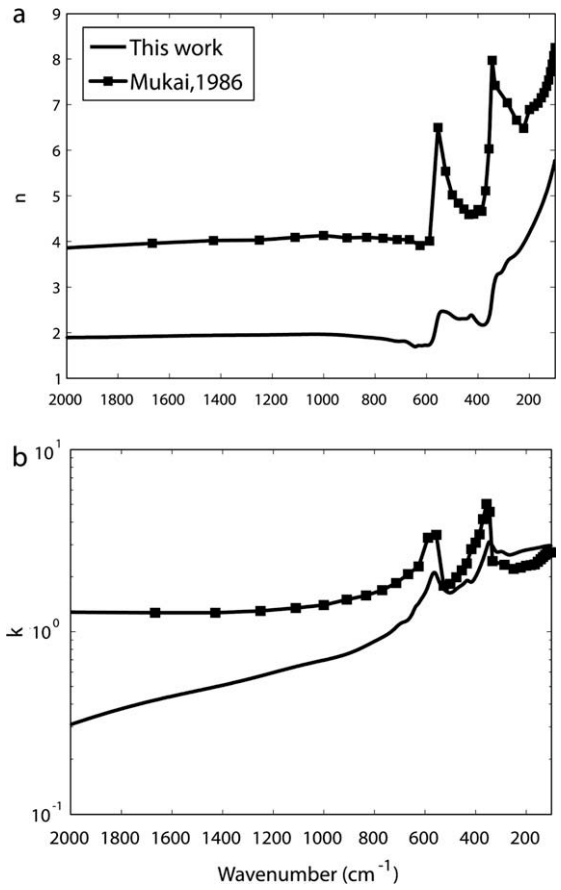

Fig. 8. Comparison of magnetite optical constants from Mukai (1986) and this work between 100 and 2000 cm^{-1}. (a) Real index (n). (b) Imaginary index (k).

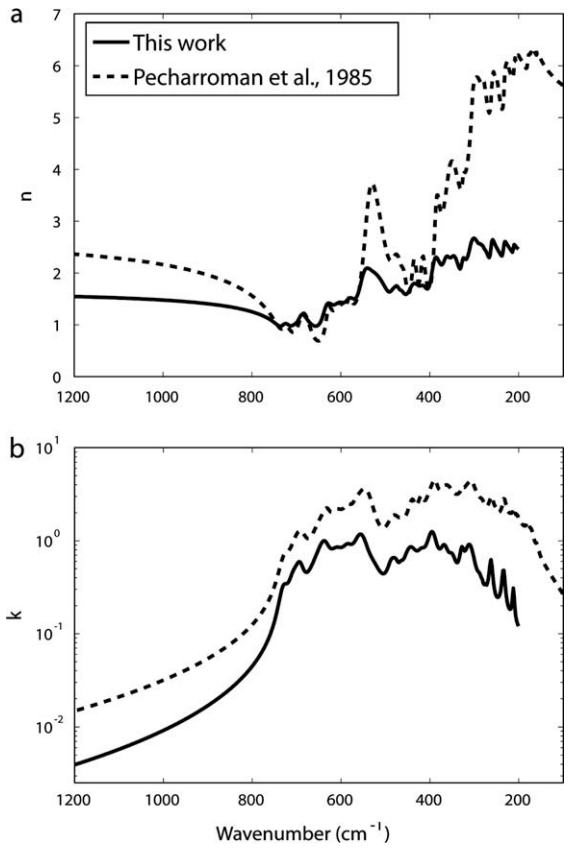

Fig. 9. Comparison of maghemite optical constants from Pecharromán et al. (1995) and this work between 100 and 1200 cm^{-1}. (a) Real index (n). (b) Imaginary index (k).

Acknowledgments

We thank Brad DeGregorio for determining the average crystal shape and size of the synthetic maghemite powder. We also thank Richard Harrington for loaning us the ferrihydrite sample and Dick Morris for loaning us the goethite and lepidocrocite samples. Karly Pitman and an anonymous reviewer provided excellent reviews that enhanced the content and clarity of the manuscript. We acknowledge NASA Mars Fundamental Research Program Grant NNX06AB20G (to GRR) and the Stony Brook University College of Arts and Sciences for funding this work.

References

Allen, C.C., Gooding, J.L., Jercinovic, M., Keil, K., 1981. Altered basaltic glass: A terrestrial analog to the soils of Mars. Icarus 45, 347–369.
Bell, J.F., Roush, T.L., Morris, R.V., 1995. Midinfrared transmission spectra of crystalline and nanophase ironoxides, oxyhydroxides, and implications for remote sensing of Mars. J. Geophys. Res. 100, 5297–5307.
Bell, J.F., and 23 colleagues, 2000. Mineralogic and compositional properties of martian soil and dust: Results from Mars Pathfinder. J. Geophys. Res. 105, 1721-1755.
Bertelsen, P., and 17 colleagues, 2004. Magnetic properties experiments on the Mars Exploration Rover Spirit at Gusev Crater. cience 305, 827-829.
Bishop, J.L., Murchie, S.L., Pieters, C.M., Zent, A.P., 2002. A model for formation of dust, soil, and rock coatings on Mars: Physical and chemical processes on the martian surface. J. Geophys. Res. 107 (E11), 5097. doi:10.1029/2001JE0011581.
Brearley, A.J., 1995. Aqueous alteration and brecciation in Bells, and unusual saponite-bearing CM chondrite. Geochim. Cosmochim. Acta 59, 2291–2317.

Brearley, A.J., 2006. The action of water. In: Lauretta, D., McSween, H.Y., Leshin, L. (Eds.), Meterorites and The Early Solar System II. University of Arizona Press, Tucson, pp. 587–624.

Clancy, R.T., Lee, S.W., Gladstone, G.R., McMillan, W.W., Roush, T., 1995. A new model for Mars atmospheric dust based upon analysis of ultraviolet through infrared observations from Mariner 9, Viking, and Phobos. J. Geophys. Res. 100, 5251–5263.

Glotch, T., Kraft, M., 2008. Thermal transformations of akaganeite and lepidocrocite to hematite: Assessment of possible precursors to martian crystalline hematite. Phys. Chem. Miner. 35, 569–581.

Glotch, T.D., Christensen, P.R., Sharp, T.G., 2006. Fresnel modeling of hematite crystal surfaces and application to martian hematite spherules. Icarus 181, 408–418.

Glotch, T.D., Rossman, G.R., Aharonson, O., 2007. Mid-infrared (5–100 μm) reflectance spectra and optical constants of ten phyllosilicate minerals. Icarus 192, 605–622.

Greenwood, N.N., 1970. Ionic Crystals, Lattice Defects, and Non-Stoichiometry. Butterworths, London. 194 pp.

Hamilton, V.E., McSween, H.Y., Hapke, B., 2005. Mineralogy of martian atmospheric dust inferred from thermal infrared spectra of aerosols. J. Geophys. Res. 110, E12006. doi:10.1029/2005JE002501.

Kandler, K., Benker, N., Bundke, U., Cuevas, E., Ebert, M., Knippertz, P., Rodriguez, S., Schutz, L., Weinbruch, S., 2007. Chemical composition and complex refractive index of Saharan Mineral Dust at Izana, Tenerife (Spain) derived by electron microscopy. Atmos. Environ. 41, 8058–8074.

Keller, L.P., Thomas, K.L., Clayton, R.N., Mayeda, T.K., Dehart, J.M., McKay, D.S., 1994. Aqueous alteration of the Bali CV3 chondrite – Evidence from mineralogy, mineral chemistry, and oxygen isotopic compositions. Geochim. Cosmochim. Acta 58, 5589–5598.

Kerridge, J.F., Mackay, A.L., Boynton, W.V., 1979. Magnetite in CI carbonaceous meteorites – Origin by aqueous activity on a planetesimal surface. Science 205, 395–397.

Koike, C., Hasegawa, H., Asada, N., Hattori, T., 1981. The extinction coefficients in mid- and far-infrared of silicate and iron-oxide minerals of interest for astronomical observations. Astrophys. Space Sci. 79, 77–85.

Landauer, R., 1978. Electrical transport and optical properties of inhomogeneous media. In: Garland, J.C., Tanner, D.B. (Eds.), Proceedings of the First Conference on the Electrical Transport and Optical Properties of Inhomogeneous Media. AIP, New York, pp. 2–45.

Lane, M.D., 1999. Midinfrared optical constants of calcite and their relationship to particle size effects in thermal emission spectra of granular calcite. J. Geophys. Res. 104, 14099–14108.

Long, L.L., Querry, M.R., Bell, R.J., Alexander, R.W., 1993. Optical properties of calcite and gypsum in crystalline and powdered form in the infrared and far-infrared. Infrared Phys. 34, 191–201.

Michel, F.M., Ehm, L., Anato, S.M., Lee, P.L., Chupas, P.J., Liu, G., Strongin, D.R., Schoonen, M.A.A., Phillips, B.L., Parise, J.B., 2007. The structure of ferrihydrite, a nanocrystalline material. Science 316, 1726–1729.

Mishchenko, M.I., Liu, L., Hovenier, J.W., 2007a. Effects of absorption on multiple scattering by random particulate media: Exact results. Opt. Express 15, 13182–13187.

Mishchenko, M.I., Liu, L., Mackowski, D.W., Cairns, B., Videen, G., 2007b. Multiple scattering by random particulate media: Exact 3D results. Opt. Express 15, 2822–2836.

Morris, R.V., Lauer, H.V., 1981. Stability of goethite (α-FeOOH) and lepidocrocite (γ-FeOOH) to dehydration by UV radiation – Implications for their occurrence on the martian surface. J. Geophys. Res. 86, 893–899.

Morris, R.V., Lauer, H.V., Lawson, C.A., Gibson, E.K., Nace, G.A., Stewart, C., 1985. Spectral and other physiochemical properties of submicron powders of hematite (α-Fe_2O_3), maghemite (γ-Fe_2O_3), magnetite (Fe_3O_4), goethite (α-FeOOH), and lepidocrocite (γ-FeOOH). J. Geophys. Res. 90, 3126–3144.

Morris, R.V., Agresti, D.G., Lauer, H.V., Newcomb, J.A., Shelfer, T.D., Murali, A.V., 1989. Evidence for pigmentary hematite on Mars based on optical, magnetic, and Mossbauer studies of superparamagnetic (nanocrystalline) hematite. J. Geophys. Res. 94, 2760–2778.

Morris, R.V., Graff, T.G., Mertzman, S.A., Lane, M.D., Christensen, P.R., 2003. Palagonitic (not andesitic) Mars: Evidence from thermal emission and VNIR spectra of palagonitic alteration rinds on basaltic rock. In: Sixth Int. Conf. Mars (abstract 3211).

Mukai, T., 1986. Cometary dust and interplanetary particles. In: Corso, C.I. (Ed.), Evolution of Interstellar Dust and Related Topics. North-Holland, Amsterdam, pp. 397–445.

Murchie, S., Kirkland, L., Erard, S., Mustard, J., Robinson, M., 2000. Near-infrared spectral variations of martian surface materials from ISM imaging spectrometer data. Icarus 147, 444–471.

Onari, S., Arai, T., Kudo, K., 1977. Infrared lattice vibrations and dielectric dispersion in a-Fe_2O_3. Phys. Rev. B 16, 1717–1721.

Pecharromán, C., Gonzalezcarreno, T., Iglesias, J.E., 1995. The infrared dielectric properties of maghemite, g-Fe_2O_3, from reflectance measurements on pressed powders. Phys. Chem. Miner. 22, 21–29.

Pollack, J.B., Colburn, D.S., Flasar, F.M., Kahn, R., Carlston, C.E., Pidek, D., 1979. Properties and effects of dust particles suspended in the martian atmosphere. J. Geophys. Res. 84, 2929–2945.

Popova, S.I., Tolstykh, T.S., Ivlev, L.S., 1973. Optical constants of Fe_2O_3 in the infrared range of the spectrum. Opt. Spectrosc. 35, 551–552.

Prospero, J.M., 1999. Long-term measurements of the transport of African mineral dust to the southeastern United States: Implications for regional air quality. J. Geophys. Res. 104, 15917–15927.

Roush, T., Pollack, J., Orenberg, J., 1991. Derivation of midinfrared (5–25 μm) optical constants of some silicates and palagonite. Icarus 94, 191–208.

Singer, R., 1982. Spectral evidence for the mineralogy of high albedo soils and dust on Mars. J. Geophys. Res. 87, 10159–10168.

Sokolik, I.N., Toon, O.B., 1999. Incorporation of mineralogical composition into models of the radiative properties of mineral aerosol from UV to IR wavelengths. J. Geophys. Res. 104, 9423–9444.

Spitzer, W.G., Kleinman, D.A., 1961. Infrared lattice bands of quartz. Phys. Rev. 121, 1324–1335.

Spitzer, W.G., Kleinman, D., Walsh, D., 1959. Infrared properties of hexagonal silicon carbide. Phys. Rev. 113, 127–132.

Tickanen, L.D., Tejedor-Tejedor, M.I., Anderson, M.A., 1997. Quantitative characterization of aqueous suspensions using variable-angle ATR-FTIR spectroscopy: Determination of optical constants and absorption coefficient spectra. Langmuir 13, 4829–4836.

Tomeoka, K., Buseck, P.R., 1988. Matrix mineralogy of the Orgueil CI carbonaceous chondrite. Geochim. Cosmochim. Acta 52, 1627–1640.

Toon, O.B., Pollack, J.B., Sagan, C., 1977. Physical properties of the particles composing the martian dust storm of 1971–1972. Icarus 3, 663–696.

Vilas, F., Jarvis, K.S., Gaffey, M.J., 1994. Iron alteration minerals in the visible and near-infrared spectra of low albedo Asteroids. Icarus 109, 274–283.

Williams, R.J., Gibson, E.K., 1972. Origin and stability of lunar goethite, hematite, and magnetite. Earth Planet. Sci. Lett. 17, 84–88.